The short duty-cycle of high redshift galaxies

J. Stuart B. Wyithe[1], Abraham Loeb[2], Pascal Oesh[3]

[1] *School of Physics, University of Melbourne, Parkville, Victoria, Australia*
[2] *Astronomy Department, Harvard University, 60 Garden Street, Cambridge, MA 02138, USA*
[3] *UCO/Lick Observatory, University of California, Santa Cruz, CA 95064, USA*
Email: swyithe@unimelb.edu.au; aloeb@cfa.harvard.edu

22 February 2013

ABSTRACT

We show that a bursty model of high redshift star formation explains several puzzling observations of the high redshift galaxy population. We begin by pointing out that the observed specific star formation rate requires a duty-cycle of $\sim 10\%$, which is much lower than found in hydro-dynamical simulations. This value follows directly from the that the observed star formation rates in galaxies integrated over a Hubble time would exceeds the observed stellar mass by an order of magnitude. We use the large observed specific star formation rate to calibrate the efficiency of feedback in a model for the high redshift star formation rate which includes merger driven star formation regulated by SNe feedback. This model reproduces the star formation rate density function and the stellar mass function of galaxies. A prediction of the model is that the specific star formation rate does not evolve with either mass or redshift as is observed. This is in contrast to results from hydrodynamical simulations where the star formation closely follows the accretion rate, and so increases strongly towards high redshift. The bursty star formation model naturally explains the observation that at $z \sim 2-4$ there is not enough stellar mass to account for all of the star-formation observed, without invoking properties like an evolving IMF. The finding of a duty cycle that is $\sim 10\%$ implies that should be ten times the number of known galaxies at fixed stellar mass that have not yet been detected. We therefore predict the existence of a large undetected population of UV-faint galaxies that accounts for most of the stellar mass density at $z = 4-8$.

Key words: galaxies: formation, high-redshift, — cosmology: theory, diffuse radiation

1 INTRODUCTION

The galaxy luminosity function is the primary observable that must be reproduced by any successful model of galaxy formation. At $z \gtrsim 6$, it also represents one of the most important observables for studying the reionization of cosmic hydrogen. The luminosity function of Lyman-break galaxy candidates discovered at $z \gtrsim 6$ in the Hubble Ultra-Deep Field is described by a Schechter function with characteristic density $\Psi_\star$ in comoving Mpc^{-3}, and a power-law slope α at luminosities L below a characteristic break $L_\star$ (e.g. Bouwens et al. 2011). Developing a theoretical picture of the important processes involved in setting the star formation rate at high redshift lies at the forefront of understanding this important cosmic epoch (e.g. Trenti et al. 2010; Finlator et al. 2011; Muñoz & Loeb 2011; Raičević et al. 2011; Salvaterra et al. 2011).

Complex hydrodynamical models have been used to model the observed properties of high redshift galaxies. For example, Finlator et al. (2011) have modelled the growth of stellar mass in high redshift galaxies using hydrodynamical simulations coupled with sub-grid models for processes including star formation and metal enrichment, and broadly reproduce the luminosity function evolution as well as the blue colours of the young stellar populations at high redshift. Similarly, Salvaterra et al. (2011) and Jaacks et al. (2012) have calculated the evolution of the luminosity function in detailed numerical simulations including calculations of enrichment and dust reddening, with the latter also including additional physics related to the transition from population-III to population-II stars. While these models are able to reproduce the luminosity function and star formation rate density function, they over-produce the high redshift stellar mass function, particularly at the low mass end.

Recently, Wyithe & Loeb (2013) presented a model for the high redshift star formation rate density function, which includes merger driven star formation regulated by SNe feedback. This model fits a range of observables, and implies
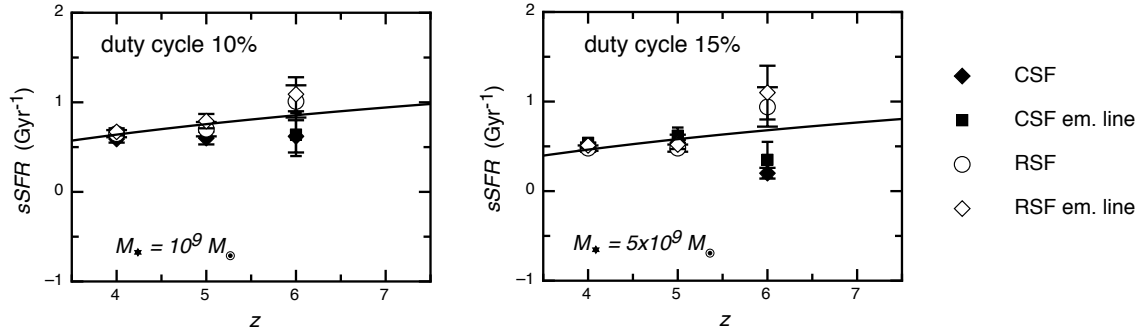
Figure 1. The specific star-formation rate as a function of redshift calculated based on equation (1) for duty-cycles of 10% and 15%, in comparison with measurements at stellar masses of 10^9 and 5×10^9 solar. The data points are from Gonzalez et al. (2012)

a duty cycle of 1-10%, much lower than found in hydro-dynamical simulations. Current observations select galaxies by their UV luminosity, and hence only detect starbursts. The finding of a duty cycle that is lower than 10% therefore implies that should be ten times the number of known galaxies at fixed stellar mass that have not yet been detected. The model therefore predicts a large undetected population of UV-faint galaxies that accounts for most of the stellar mass density at z=4-8. Unfortunately, at $z > 4$ there are currently no good constraints on non star-forming galaxies. These UV faint galaxies would be detectable with However, it is difficult to define selection criteria that select such sources without significant contamination from lower redshift dusty galaxies. The existence of a large population of undetected galaxies which are not forming stars would not affect the global star formation rate history or inferences about the reionization of the IGM, but would affect the estimated cumulative stellar mass as a function of redshift and the number density of passive galaxies at each redshift.

The relationship between the observed star formation and stellar mass, has been an observational focus. Wilkins et al. (2008) compiled estimates of stellar mass and star formation rates as a function of redshift in order to investigate whether the integral of star formation rate matches the the observed stellar mass. Interestingly, at $z \sim 2 - 4$, Wilkins et al. (2008) find that there is not enough stellar mass to account for all of the star-formation observed. Conversely, at high redshift Bouwens et al. (2011) find that the observed stellar mass is accounted for by the observed star-formation rate. In this paper we argue that both observations can be understood in the context of a star formation model with a duty-cycle of order 10%.

A second puzzling observation in high redshift galaxy research has been that the star formation rate does not evolve with either mass or redshift. Most simulations of high redshift galaxy formation do not reproduce the observed plateau in specific star formation rate at $z > 2$. This is because simulations generally associate star formation primarily with the accretion of gas. As a result they predict a rapid increase in the specific star formations rate, which can be understood because the specific accretion rate is found to scale as $(1 + z)^{2.5}$ (Neistein & Dekel 2008). To understand which aspect of high redshift galaxy formation models drives the incorrect prediction of an evolving specific star formation rate, Weinmann et al. (2011) calculated the spe-

cific star formation history within a suite of semi-analytic models. At $z > 4$, they found that the evolution of specific star formation rate could be reproduced in the presence of strong SNe feedback. In this paper, we find that SNe regulated model with low duty cycle naturally reproduces both the large value of specific SFR, and the observed behaviour with mass and redshift.

We begin in § 1 by pointing out the general constraint on the duty-cycle that is provided by observations of the specific star formation rate. Then, in § 3 we briefly summarize the formation presented in Wyithe & Loeb (2013). We next present comparison of this model with various observables including the star formation rate density function, specific star formation rate, clustering amplitude and stellar mass function in § 4. We finish with a discussion in § 5. In our numerical examples, we adopt the standard set of cosmological parameters (Komatsu et al. 2011), with values of $\Omega_\mathrm{b} = 0.04$, $\Omega_\mathrm{m} = 0.24$ and $\Omega_\Lambda = 0.76$ for the density parameters of matter, baryon, and dark energy, respectively, $h = 0.73$, for the dimensionless Hubble constant, and $\sigma_8 = 0.82$.

2 THE SPECIFIC STAR FORMATION RATE OF STAR-FORMING GALAXIES

Before discussing our particular model for SNe regulated star formation, we begin by looking at the constraint on duty-cycle (ϵ_duty) pr rate. In the simplest model the specific star formation rate is

$$sSFR = \frac{SFR}{M_\mathrm{star}} = \frac{SFR}{SFR(\epsilon_\mathrm{duty} H^{-1})^{-1}} = \epsilon_\mathrm{duty} H^{-1}. \quad (1)$$

Thus, the specific star formation rate leads to a direct estimate of the duty cycle of star formation. This is plotted in the upper two panels of Figure 1 as a function of redshift for $\epsilon_\mathrm{duty} = 0.1$ and 0.15, compared with observations of specific star formation rate at stellar masses of $M_\star = 10^9 \mathrm{M}_\odot$ and $M_\star = 5 \times 10^9 \mathrm{M}_\odot$ respectively. We note the weak dependence of the inferred duty-cycle over the range of stellar mass and redshift probed. This low duty cycle has a range of important implications for the properties of the high redshift galaxy population, and several puzzling properties of the observed relation between stellar mass and

star formation rate. For the remainder of this paper we explore these explanations in the context of the merger driven model of Wyithe & Loeb (2013).

3 MODEL

A complication that arises when modelling the luminosity function is that models predict a star formation rate, which must then be converted to a luminosity assuming an initial mass function (IMF) for the stars. While this calculation is straightforward, of more importance is the potential contribution of reddening. A simpler way to constrain theory by observations is therefore to estimate the star formation rate density observationally, where the correction is made from luminosity to star formation rate using the observed continuum properties of the galaxies under study. Recently, this has become a viable approach following the work of Smit et al. (2012) who combined estimates of dust extinction at $z \sim 4 - 7$ with measurements of the UV luminosity function in order to derive star formation rate density (SFRD) functions at $z \sim 4$, 5, 6 and 7. The resulting star formation rate density (SFRD) functions are well-described by a Schechter function, with a characteristic break separating a shallow dependence of SFRD on star formation rate at low luminosities from the exponential dependence at high luminosities. We focus on modelling the SFRD function rather that the luminosity function of high redshift galaxies.

In this section be briefly summarise the model for star formation in high redshift galaxies presented in Wyithe & Loeb (2013). The reader is referred to that paper for details of this model. The star formation rate in a galaxy halo of mass M that turns a fraction $f_\star$ of its disk mass $m_d M$ into stars over a time t_{SF} is

$$SFR = 0.15 \mathrm{M}_\odot \mathrm{yr}^{-1} \left(\frac{m_\mathrm{d}}{0.17} \right) \left(\frac{f_\star}{0.1} \right) \left(\frac{M}{10^8 \mathrm{M}_\odot} \right) \left(\frac{t_{SF}}{10^7 \mathrm{yr}} \right)^{-1}. \tag{2}$$

The model assumes that major mergers trigger bursts of star formation. The star formation rate density function (i.e. galaxies per Mpc^{-3} per unit of SFR) can be estimated as

$$\Phi(SFR) =$$
$$\epsilon_\mathrm{duty} \left(\Delta M \, t_\mathrm{H} \frac{dN_\mathrm{merge}^2}{dt d\Delta M} \bigg|_{M_1, \Delta M} \frac{dn}{dM} \right) \left(\frac{dSFR}{dM} \right)^{-1}, \tag{3}$$

where ϵ_duty is the fraction of the Hubble time (t_H) over which each burst lasts, and dn/dM is mass function of dark matter halos (Press & Schechter 1974; Sheth & Tormen 1999). The rate of major mergers (dN_merge/dt) is calculated as the number of halos per logarithm of mass ΔM per unit time that merge with a halo of mass M_1 to form a halo of mass M (Lacey & Cole 1993). We assign a 2:1 mass ratio to major mergers (i.e. $M_1 = \frac{2}{3} M$ and $\Delta M = M/3$).

The most massive stars fade away on a timescale of $t_\mathrm{s} \sim 3 \times 10^6$ years (Barkana & Loeb 2001). If the starburst lifetime t_{SF} is the duty-cycle can be written as

$$\epsilon_\mathrm{duty} = \frac{t_\mathrm{s} + t_{SF}}{t_\mathrm{H}}. \tag{4}$$

For comparison with observations we define

$$\Psi(SFR) = \ln 10 \times SFR \times \Phi, \tag{5}$$

which has units of Mpc^{-3} per dex.

We expect that SNe feedback will alter the fraction of gas in a galaxy that is turned into stars (e.g. Dekel & Woo 2003). To determine the mass and redshift dependence of $f_\star$ in the presence of SNe we suppose that stars form with an efficiency $f_\star$ out of the gas that collapses and cools within a dark matter halo and that a fraction F_SN of each supernova energy output, E_SN, heats the galactic gas mechanically (allowing for some losses due to cooling). The mechanical feedback will halt the star formation once the cumulative energy returned to the gas by supernovae equals the total thermal energy of gas at the virial velocity of the halo (e.g. Wyithe & Loeb 2003). Hence, the limiting stellar mass is set by the condition

$$\frac{M_\star}{w_\mathrm{SN}} E_\mathrm{SN} F_\mathrm{SN} f_\mathrm{t} f_\mathrm{d} = E_\mathrm{b} = \frac{1}{2} m_\mathrm{d} M v_\mathrm{vir}^2. \tag{6}$$

In this relation E_b is the binding energy in the halo, w_SN is the mass in stars per supernova explosion, and the total stellar mass is $M_\star = m_\mathrm{d} M f_{\star,\mathrm{tot}}$ where $f_{\star,\mathrm{tot}} = N_\mathrm{merge} f_\star$ is the total fraction of the gas that is converted to stars during major mergers, and N_merge is the number of major mergers per Hubble time. The parameters f_t and f_d denote the fraction of the SNe energy that contributes because of the finite timescale of the SNe feedback or the disk scale height being smaller than the SNe bubble. These terms are described in more detail below.

The ratio between the total mass in stars and dark matter is observed to increase with halo mass as $(M_\star/M) \propto M^{0.5}$ for $M_\star \lesssim 3 \times 10^{10} \mathrm{M}_\odot$, but is constant for larger stellar masses (Kauffmann et al. 2003). Thus, the star formation efficiency within dwarf galaxies decreases towards low masses. For comparison with equation (6), a Scalo (1998) mass function of stars has $w_\mathrm{SN} \sim 126$ M$_\odot$ per supernova and $E_\mathrm{SN} = 10^{51}$ ergs, and so we find that $M_\star = 3 \times 10^{10}$ M$_\odot$ and $v_\mathrm{c} \sim 175$ km/s (the typical value observed locally; see e.g. Bell & de Jong 2001) implies $f_{\star,\mathrm{tot}} \sim 0.1$ for a value of $F_\mathrm{SN} \sim 0.5$. Smaller galaxies have smaller values of $f_\star$. Equation (6) indicates that

$$f_\star =$$
$$\min \left[f_{\star,\mathrm{max}}, \frac{0.008}{N_\mathrm{merge}} \left(\frac{M}{10^{10} \mathrm{M}_\odot} \right)^{\frac{2}{3}} \left(\frac{1+z}{10} \right) (f_\mathrm{t} f_\mathrm{d} F_\mathrm{SN})^{-1} \right] \tag{7}$$

We utilise equation (7) with equation (3) as a function of the parameters t_{SF} and $f_{\star,\mathrm{max}}$.

3.1 Disk structure

The effect of SNe feedback is dependent on the conditions of the interstellar medium (ISM) gas. We assume that the cold gas (out of which stars form) occupies a self-gravitating exponential disk where R_d is the scale radius, m_d is the mass fraction of the disk relative to the halo and $\lambda \sim 0.05$ is the spin parameter of the halo (Mo et al. 1998). The scale height of the disk at radius r is

$$H = \frac{c_\mathrm{s}^2}{\pi G \Sigma(r)}, \tag{8}$$

where c_s is the sound speed in the gas, which we assume to have a temperature of 10^4K, and $\Sigma(r)$ is the surface density. We adopt the density in the mid plane at the scale radius,
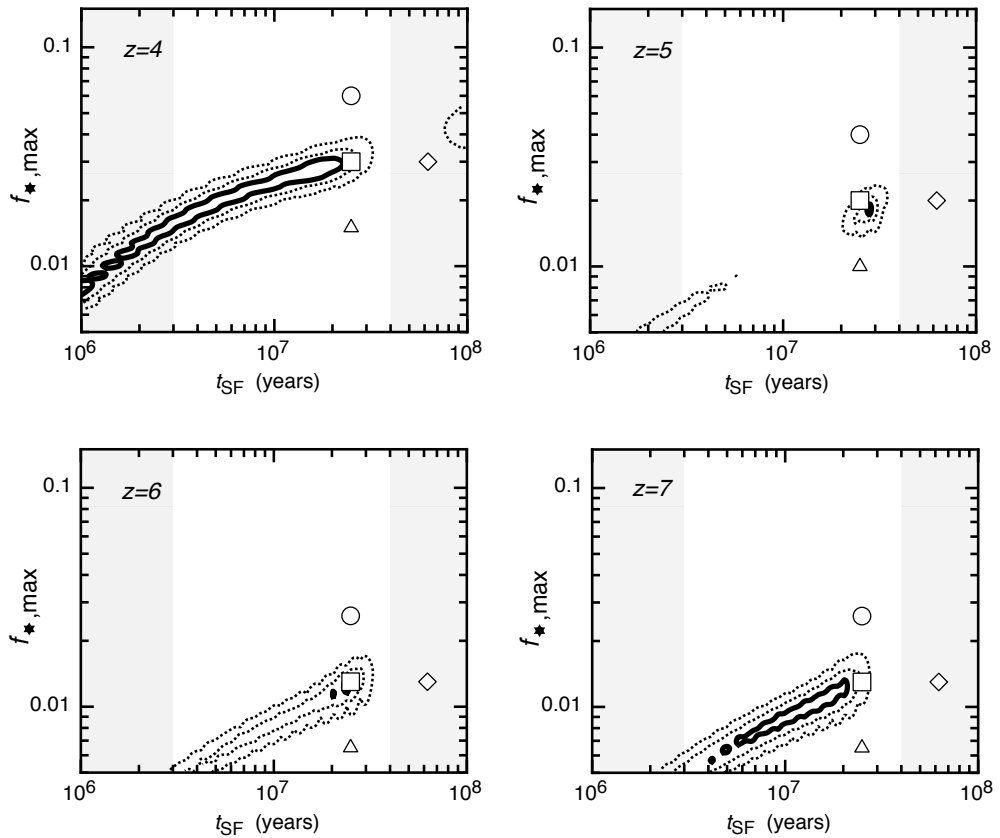
Figure 2. Constraints on the model parameters $f_{\star,\mathrm{max}}$ and t_{SF} at four different redshifts (constraints are independent at each redshift). In each case, three contours are shown corresponding to differences in χ^2 relative to the best-fitting model of $\Delta\chi^2 = \chi^2 - \chi^2_{\mathrm{min}} = 1$, 2.71 and 6.63. Projections of these contours on to the axes provide the 68.3, 90 and 99 per cent confidence intervals on individual parameter values. The vertical grey regions represent time-scales longer/shorter than the lifetime of the highest/lowest mass SNe progenitor ($3 \times 10^6\,\mathrm{yr}/4 \times 10^7\,\mathrm{yr}$).

within which half the gas is contained, as representative of the density of the ISM.

3.2 Supernova evacuation of the ISM

Clarke & Oey (2002) presented a simple analytic model for the effect of supernovae on the interstellar medium which we apply to high redshift galaxies. In this model, clusters of N_e SNe produce super-bubbles in the ISM with a radius R_e at which the super-bubble comes into pressure balance with the ISM. This radius can be found by approximating R_e as the radius within which the thermal energy of the ISM equals the mechanical energy of the SNe cluster. The timescale associated with the evacuation of a super bubble in the ISM by a SNe cluster is $t_e = 4 \times 10^7$ years, corresponding to the lifetime of the lowest mass SNe progenitor. The evacuation radius for a cluster of N_e SNe, each with energy output E_{SN} within an ISM of sound speed c_s is

$$
\begin{aligned}
R_e = {} & 0.08\,\mathrm{kpc} \left(\frac{N_e}{10}\right)^{\frac{1}{3}} \left(\frac{E_{\mathrm{SN}}}{10^{51}\mathrm{erg}}\right)^{\frac{1}{3}} \left(\frac{\lambda}{0.05}\right)^{\frac{4}{3}} \left(\frac{m_d}{0.17}\right)^{-\frac{2}{3}} \\
& \times \left(\frac{M}{10^8 \mathrm{M_\odot}}\right)^{-\frac{2}{9}} \left(\frac{1+z}{10}\right)^{-\frac{4}{3}}.
\end{aligned} \tag{9}
$$

In the limit where SNe evacuated regions are smaller than the scale height of the disk, and the starburst lifetime t_{SF} is much larger than the gas evacuation timescale t_e, the fraction F_{SN} of the SNe energy may be used in feedback suppressing subsequent star formation. However, if the SNe evacuated regions break out of the disk, or $t_{\mathrm{SF}} < t_e$, not all of the energy will be available for feedback. Based on the ISM porosity model of Clarke & Oey (2002), a fraction $f_d = 2H/R_e$ of the SNe energy goes to increasing the ISM porosity for disks where $R_e > H$. In this case we find

$$
\begin{aligned}
f_d = {} & 0.85 \left(\frac{N_e}{10}\right)^{-\frac{1}{3}} \left(\frac{E_{\mathrm{SN}}}{10^{51}\mathrm{erg}}\right)^{-\frac{1}{3}} \left(\frac{\lambda}{0.05}\right)^{\frac{2}{3}} \left(\frac{m_d}{0.17}\right)^{-\frac{1}{3}} \\
& \times \left(\frac{M}{10^8 \mathrm{M_\odot}}\right)^{-\frac{1}{9}} \left(\frac{1+z}{10}\right)^{-\frac{2}{3}} \left(\frac{c_s}{10\mathrm{km/s}}\right)^2, \quad (10)
\end{aligned}
$$

as long as $f_d < 1$ and $f_d = 1$ otherwise. Similarly, in cases where $t_{\mathrm{SF}} < t_e \sim 4 \times 10^7$ yrs, only

$$
f_t \equiv (t_{\mathrm{SF}}/t_e)^2 \tag{11}
$$

of the overall SNe energy output is generated by the time the starburst concludes. The quadratic dependence on time arises because the number of bubbles produced grows in proportion to time, while the maximum size of a bubble at
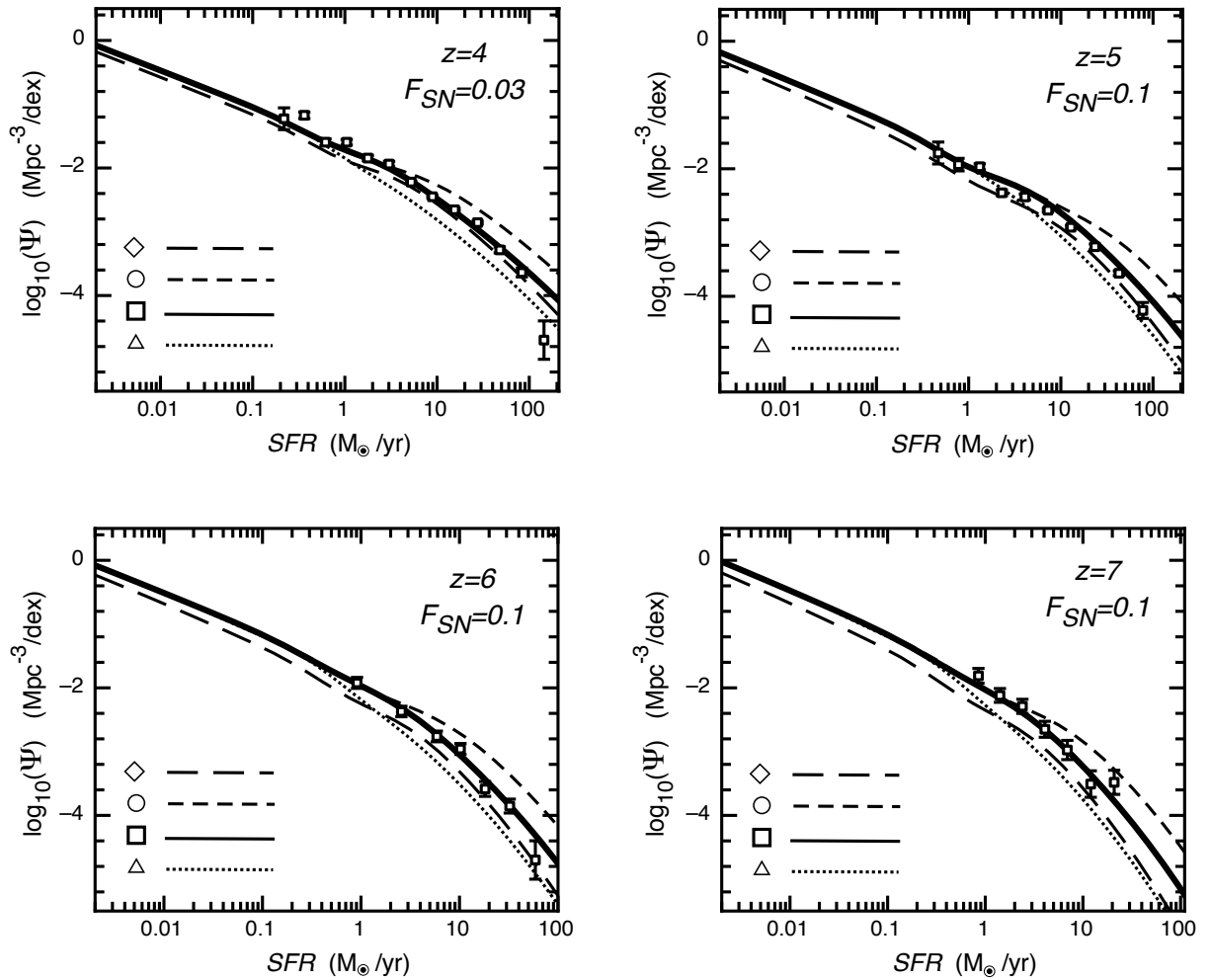
Figure 3. Comparison between the observed and modelled SFRD function (plotted as $\Psi = \ln 10 \times SFR \times \Phi$). The four panels show results for different redshift values. In each panel, the four curves correspond to a different choice of model parameters t_{SF} and $f_{\star,\mathrm{max}}$, labeled by the symbols in Figure 2. The thick solid lines represent values close to the best fit.

time $t < t_e$ is also proportional to time (Oey & Clarke 1997). In cases where $t_{\mathrm{SF}} > t_e$ we have $f_t = 1$.

4 RESULTS

The inferred duty cycle based on Figure ?? is much lower than unity, but is larger than the value found in the merger driven model of Wyithe & Loeb (2013). We note that there is degeneracy in the model between between duty-cycle ϵ_{duty} and the parameter F_{SN} which governs the fraction of SNe energy that is harnessed for feedback. In Wyithe & Loeb (2013) we simply chose an arbitrary value for this since it is unconstrained by just the SFR density function. However, including the constraint on specific star formation rate allows us to constrain F_{SN} in addition to $f_{\star,\mathrm{max}}$ and t_{SF}. In the following section we use this additional constraint.

4.1 Comparison with observations

We fit our model to the recent data of Smit et al. (2012) in order to constrain the two free parameters of our star formation model t_{SF} and $f_\star$ separately for four different redshifts $z \sim 4, 5, 6$ and 7. Specifically we use the model to calculate SFRD functions for combinations of these parameters and calculate the χ^2 of the model as

$$\chi^2(f_{\star,\mathrm{max}}, t_{\mathrm{SF}}) =$$
$$\sum_{i=0}^{N_{\mathrm{obs}}} \left(\frac{\log \Psi(SFR_i, f_{\star,\mathrm{max}}, t_{\mathrm{SF}}, z) - \log \Psi_{\mathrm{obs}}(SFR_i, z)}{\sigma_{SFR}(SFR_i, z)} \right)^2 (12)$$

Here $\Psi_{\mathrm{obs}}(SFR_i, f_{\star,\mathrm{max}}, t_{\mathrm{SF}}, z)$ is the observed star formation rate density measured at redshift z, with uncertainty in dex of $\sigma_{SFR}(SFR_i)$. In calculating likelihoods at $z \sim 4$ and $z \sim 5$ we increased the quoted error bars by factors of 3 and 2 respectively in order to obtain a reduced χ^2 of order unity. The SFRD function is sensitive to the value of F_{SN}, and we therefore integrate the likelihood over a range
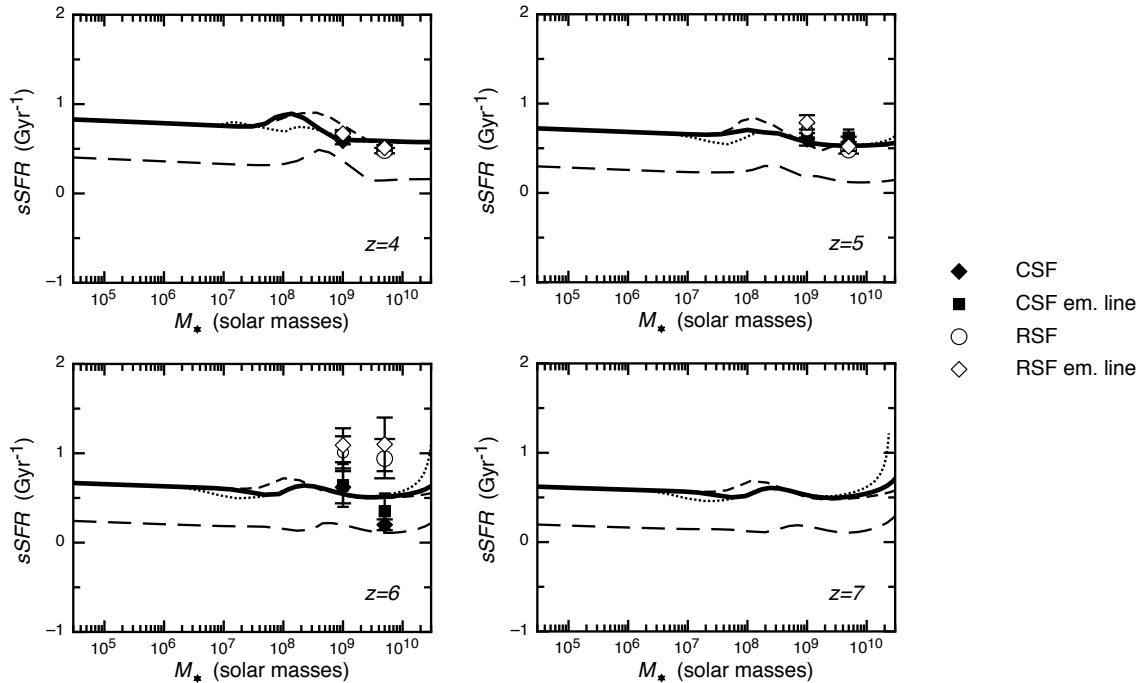
Figure 4. The specific star-formation rate for these models as a function of stellar mass (as predicted by the star-burst only model). The data points are from Gonzalez et al. (2012).
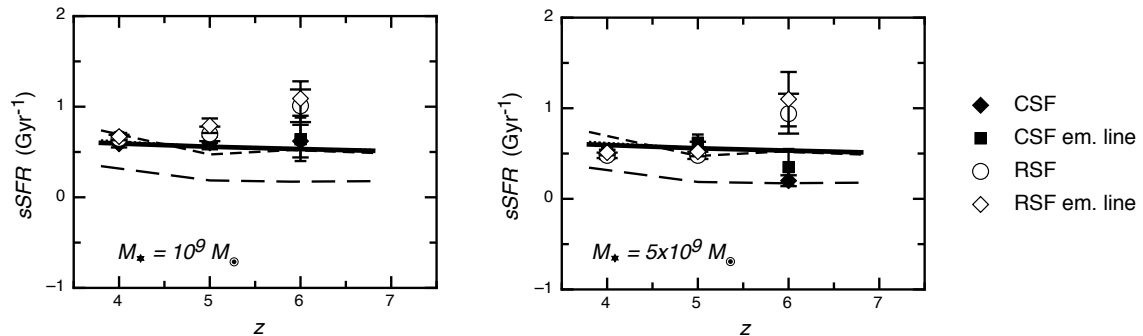
Figure 5. The specific star-formation rate as a function of redshift for stellar masses of 10^9 and 5×10^9 solar masses. The data points are from Gonzalez et al. (2012).

of values uniformly distributed between $-1 < \log_{10} F_{\rm SN} < 0$

$$\mathcal{L}(f_{\star,\max}, t_{\rm SF}) \propto \int_{-1}^{0} d(\log_{10} F_{\rm SN}) e^{-\chi^2/2}. \qquad (13)$$

We note that the relation between SFR and M in equation (2) is not perfect. As part of our comparison with observations, and to account for scatter in this relationship, we convolve the predicted SFRD function equation (3) with a Gaussian of width 0.5 dex in SFR. An intrinsic scatter of 0.5 dex is motivated by the scatter in stellar mass at constant SFR found by González et al. (2011). However, in addition we find that the value of 0.5 dex provides the best statistical fit to the observations. Our qualitative results are not sensitive to the choice of this scatter.

4.2   Parameter constraints

In Figure 2 we show constraints on models models for values of $F_{\rm SN} = 0.03$ at $z = 4$ and $F_{\rm SN} = 0.1$ at $z = 5, 6$ and 7 (c.f. $F_{\rm SN} = 0.1$ and 0.3 in the original paper). Given these sSFR driven constraints on $F_{\rm SN}$, we find that the shape of the SFRD function requires starburst durations of a few tens of Myr at $z \sim 5$, $z \sim 6$ and $z \sim 7$, with a few percent of the gas turned into stars per burst. For comparison the left and right hand vertical grey regions represent times smaller than the lifetime of the most massive stars ($t_{\rm s} \sim 3 \times 10^6$ years), and times in excess of the lifetime of the least massive stars that produce SNe respectively. Our results therefore indicate that star formation in high redshift galaxies is terminated on the same timescale as feedback from SNe can be produced (Wyithe & Loeb 2013).
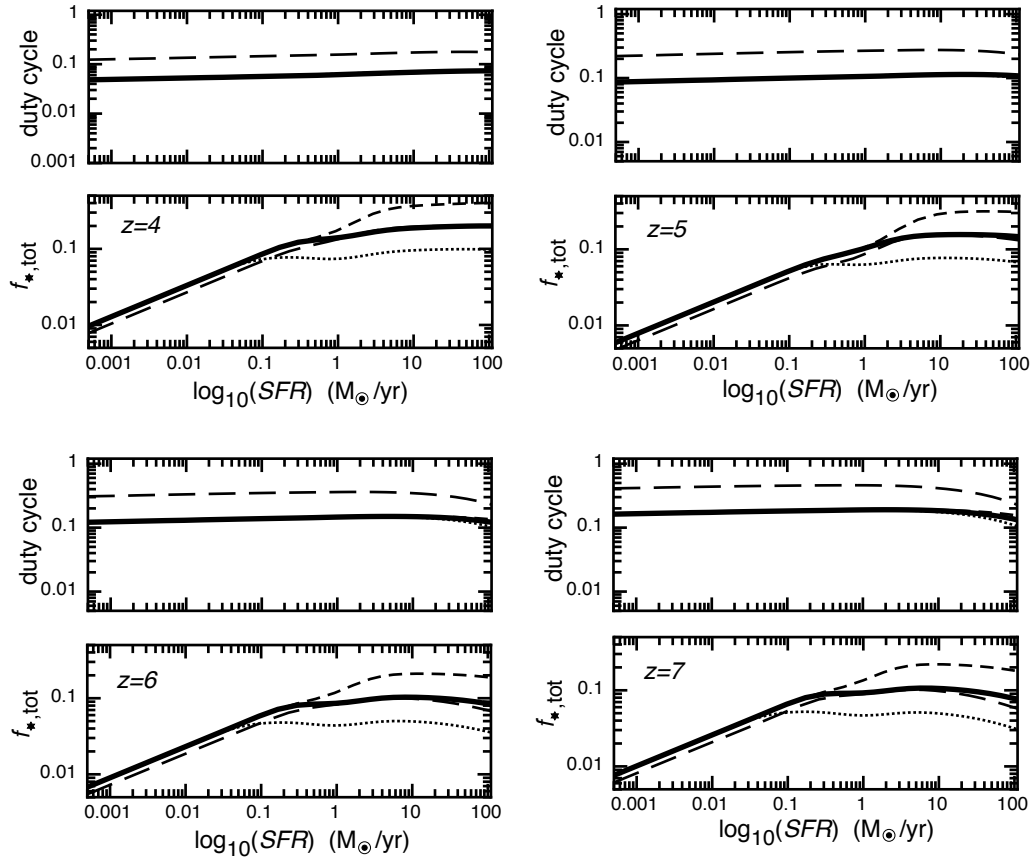
Figure 6. The values of total star formation efficiency $f_{\star,\text{tot}}$ (i.e. the sum of $f_\star$ over all mergers), and the overall duty-cycle (i.e. the fraction of a Hubble time during which a galaxy is starbursting) as a function of SFR. The four curves shown correspond to the SFRD functions shown in Figure 3, with model parameters t_{SF} and $f_{\star,\text{max}}$ designated by the symbols in Figure 2.

Figure 3 shows the comparison between observed and modelled SFRD functions for four different redshifts $z \sim 4$, 5, 6 and 7. The burst lifetime is $t_{\text{SF}} = 2.5 \times 10^7$ years in each case. The four curves shown correspond to model parameters t_{SF} and $f_{\star,\text{max}}$ labeled by the symbols in Figure 2. The thick solid lines show models close to the best fit to the observational data[1]. The other three values were chosen so as to illustrate the dependence of the predicted SFRD function on the different parameters.

Figure 4 shows the specific star formation rate as a function of mass for the models listed in Figure 3 at $z = 4, 5, 6$ and 7, illustrating the success of the model in reproducing the observed specific star formation rate for the constrained parameters (particularly F_{SN}). Beyond the narrow range of observed stellar mass values, the model predicts that the specific star-formation rate remains quite insensitive to stellar mass (or star formation rate). Figure 5 shows the specific star formation rate as a function of redshift for these models, illustrating the model prediction that the specific star-

formation rate does not evolve with redshift. This finding is in agreement with observations, in contrast to results from many hydrodynamical, models of galaxy formation indicating that star formation activity does not directly follow the gas accretion rate.

The parameters $f_{\star,\text{max}}$ and t_{SF} refer to single bursts, whereas our model includes multiple bursts at the rate of major mergers. We therefore calculate the total star formation efficiency $f_{\star,\text{tot}} = N_{\text{merge}} f_\star$ (i.e. the sum of $f_\star$ over all mergers), as well as the overall duty-cycle $\epsilon_{\text{duty,tot}} = N_{\text{merge}} t_{\text{SF}}/t_{\text{H}}$. These quantities are plotted in Figure 6 based on our model with parameter choices corresponding to the examples in Figure 3. We find that $\sim 5-10\%$ of the gas forms stars in bright galaxies of $SFR \sim 1-100\text{M}_\odot$ per year, with lower fractions down to a percent in fainter galaxies. We find duty-cycles of $\sim 10-20$ %, with higher duty-cycles at higher redshift reflecting the increased ratio between the lifetime of massive stars and the age of the Universe. The duty cycle is also larger for systems of higher star formation rate. This trend is in agreement with the observational estimate of Lee et al. (2009) based on comparison of the luminosity and clustering of luminous $z \gtrsim 4$ galaxies. These authors (see also Lee et al. 2012) find that star-formation is constrained

---

[1] These curves are not plotted at the formal best fit because whereas the constraints were determined independently, we have chosen common values for parameters $f_{\star,\text{max}}$ and t_{SF} across several redshifts.
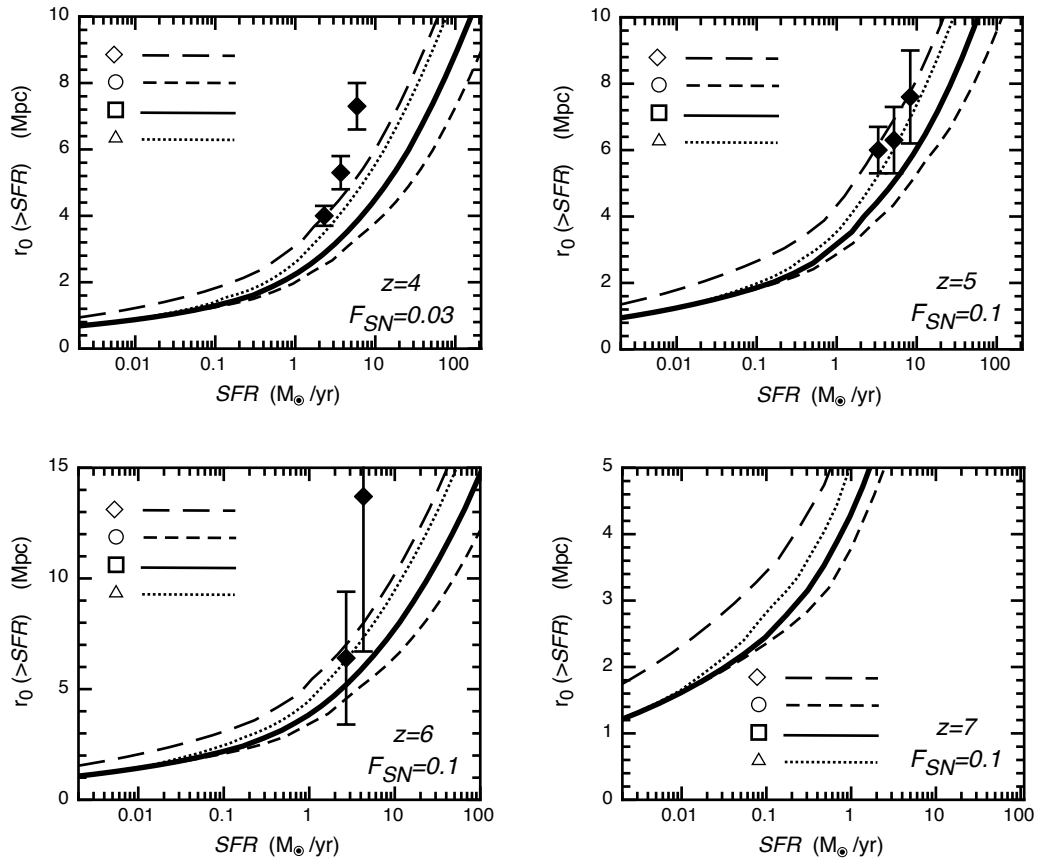
Figure 7. The correlation length in samples above a limiting SFR. The data points are from Lee+09 and Overzier+06. I calculated the correlation length for a sample above the limiting star-formation rate by averaging over correlation functions weighted by the SFR density function

to be bursty, and infer a duty-cycle at $z \sim 4$ (15%-60% at 1-σ).

4.3   Clustering of star forming galaxies

To check whether the relationship between halo mass and SFR is correctly reproduced in our model we calculate the correlation length in samples above a limiting SFR for the four models in this paper. The results are plotted in Figure 7. The correlation length is calculated for a sample above the limiting star-formation rate by averaging over correlation functions weighted by the SFR density function. For comparison we also include clustering measurements from Lee et al. (2009) and Overzier et al. (2006). To convert from an apparent magnitude limit to an intrinsic star formation rate, we assumed a flat SED with $\beta = -2$ for computation of a K-correction, and a conversion conversion from UV luminosity to SFR using Kennicutt (1998). We find that the clustering length increases rapidly towards high SFRs, in agreement with observations. Our model yields a clustering length in the best fit model is consistent with clustering measurements at $z \sim 5 - 6$, but underestimates observations at $z \sim 4$.

4.4   The stellar mass function

The final observable that we consider is the stellar mass function. Observationally, the stellar mass function that is observed is the stellar mass function of Ly-break selected galaxies, which can be estimated as

$$\Theta(M_\star) = \Phi(SFR) \times \left(\frac{dSFR}{dM_\star} \right) = \Phi(SFR) \times sSFR. \quad (14)$$

The resulting stellar mass function is plotted as the green curves in Figure 8 for the models shown in Figure 3-7. The data points are from González et al. (2011). Since since the model produces both the correct specific star formation rate and the SFR density function it is no surprise that the agreement is good. This agreement is in contrast to most hydrodynamical models of galaxy formation, in which the constant accretion leads to high duty cycles mean that the SFR to halo mass is too low. This low mass-to-light ratio is why hydrodynamical models lead to a mass function that is too steep.

The low duty-cycle implies that our model predicts the existence of many galaxies of large stellar mass that are not star forming, and so not included in the Ly-break selected stellar mass function. Using our model we therefore calculate the predicted mass function in the case where the sample

ratio
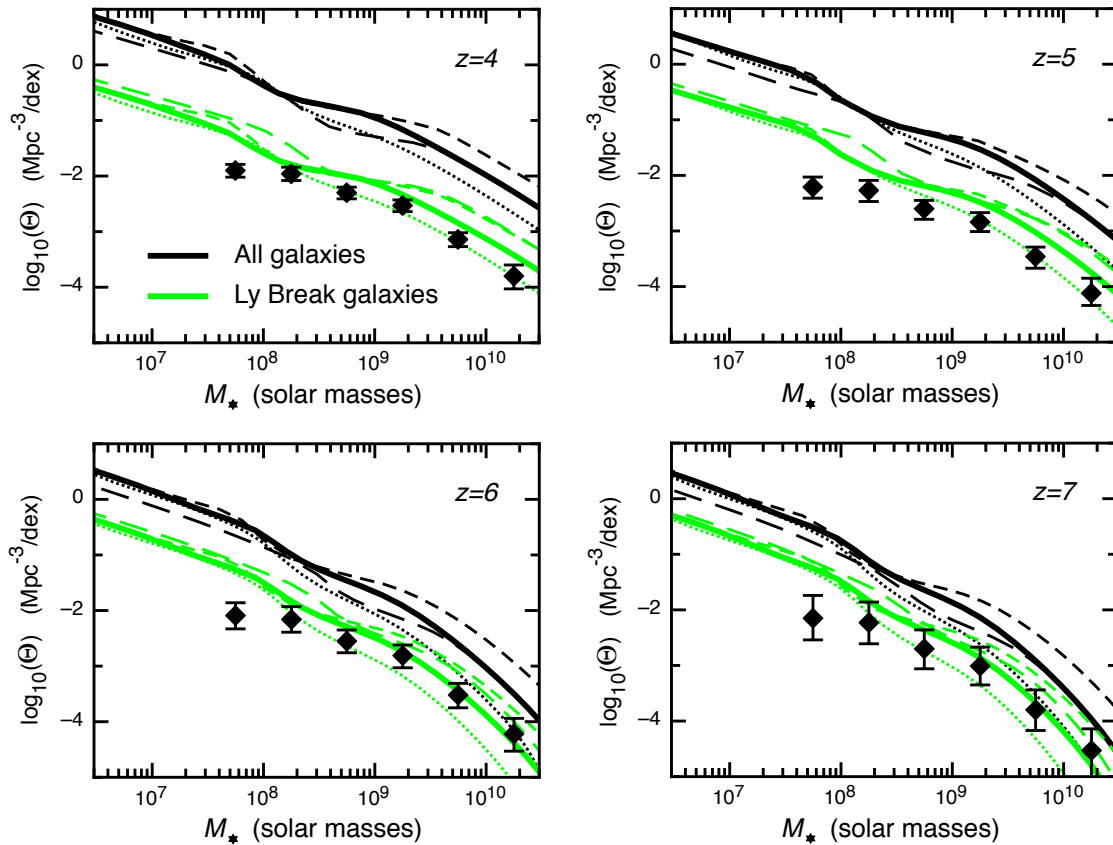
Figure 8. The stellar mass function of a Ly-break selected sample. This is plotted as the green curves in the attached figure. These curves are for the same models as Figures 3-7. The data points are from González et al. (2011). We also calculate the mass function that would be seen if the sample were selected in stellar mass rather than SFR. The black curves show these models, which are a factor of 5 to 10 higher.

were selected in stellar mass rather than SFR. This is

$$
\begin{aligned}
\Theta_{\mathrm{all}}(M_\star) &= \frac{1}{\epsilon_{\mathrm{duty,tot}}} \Phi(SFR) \times \left(\frac{dSFR}{dM_\star} \right) \\
&= \frac{1}{\epsilon_{\mathrm{duty,tot}}} \Phi(SFR) \times sSFR \\
&= \frac{1}{\epsilon_{\mathrm{duty,tot}}} \times \Theta(M_\star).
\end{aligned}
\tag{15}
$$

In Figure 8 we show the resulting predicted stellar mass functions for the models shown in Figure 3-7 (black curves). Owing to the low duty-cycle, these curves are a factor of 5 to 10 higher than the Ly-break selected case, indicating that high redshift surveys miss most of the stellar mass produced

Add a section (best if written by Pascal) about how to detect the missing population of galaxies with Spitzer, HST or JWST.

5 DISCUSSION

In this paper we have employed a bursty model for SNe regulated high redshift star formation to investigate possible solutions to two observed puzzles in high redshift galaxy formation.

The first puzzle relates to the issue of an observed specific star-formation rate that does not evolve with redshift, in contrast to theoretical expectation. The shape of the stel-

lar mass function for high redshift galaxies is related to this quantity. We find that the value of the specific star formation rate, and its observed evolution at high redshift directly constrain the duty-cycle of high redshift star-formation to be approximately 10%, independent of a specific model for star-formation.

The second puzzle lies in the relation between the observed growth of stellar mass and the observed instantaneous star formation rate. The observed stellar mass density that is directly observed in samples at high redshift is the stellar mass density in the population of star forming galaxies rather than the total stellar mass density in the Universe (González et al. 2011). Our model successfully reproduces this star-formation selected stellar mass because it predicts the correct specific star formation rate. However, if we are considering the stellar mass function of the whole galaxy population then there is stellar mass missing from the observed census. Moreover, there seems to be disagreement between the relation of star formation rate to stellar observed at $z \sim 6$ (Bouwens et al. 2011) and $z \sim 2 - 4$ (Wilkins et al. 2008).

Specifically, at $z \sim 2 - 4$, Wilkins et al. (2008) find that there is not enough stellar mass to account for all of the star-formation observed. Wilkins et al. (2008) calculate the stellar mass using fits to the stellar mass function, extrapo-

lated to high and low mass, and then find the star formation rate as the derivative of this function. If the observed star formation rate is $\dot{\rho}_{\star,\mathrm{obs}}$ in units of mass per time per Mpc^3, we can calculate the inferred stellar mass density as

$$\rho_{\star,\mathrm{inf}} = \dot{\rho}_{\star,\mathrm{obs}}\frac{dt}{dz}\Delta z, \qquad (16)$$

where $\Delta z \sim 0.5$ is the survey depth. When this is compared with the observed stellar mass density at $z \sim 2-4$, $\rho_{\star,\mathrm{obs}}$, Wilkins et al. (2008) found that $\rho_{\star,\mathrm{obs}} < \rho_{\star,\mathrm{inf}}$ with a difference of ~ 0.6 dex. However with a duty-cycle smaller than unity, the stellar mass in the star forming galaxies was built up over a time shorter than the survey depth, meaning that $\rho_{\star,\mathrm{inf}}$ is an overestimate relative to the observed stellar mass. In this case only a fraction ϵ of galaxies with stellar mass $M_\star$ are observed in a particular survey, but all galaxies would have starbursts during a time corresponding to the survey depth (note this does not imply that the instantaneous SFRD is underestimated). Thus, if a Ly-break is needed to find the galaxies, much of the stellar mass at a particular time is contained in non-star forming galaxies and so would be missed by the survey (by a factor of inverse the duty-cycle), explaining the difference found by Wilkins et al. (2008).

In a complementary analysis Bouwens et al. (2011) have taken the stellar mass function at $z \sim 6-8$ determined by González et al. (2011) and differentiated to get the star formation rate in a survey at $z > 6$. However in this higher redshift case, the resulting stellar mass is found to agree better with the stellar mass inferred directly from spectroscopy, in contrast to the results of Wilkins et al. (2008) at $z \sim 2-4$. At first sight this is a failure for our model, which predicts that these estimates differ by a factor of inverse duty-cycle as they do at lower redshift. The solution to this apparent contradiction lies in the fact that the survey depth of $\Delta z \sim 0.5$ corresponds to a time difference across the survey that is longer than the star-burst lifetime at $z \sim 2-4$, but similar to the starburst lifetime at $z \sim 6-8$. This means that at $z \sim 2-4$, the observed galaxies do not form stars for a time that is as long as the duration of the survey, implying that the contribution to the stellar mass from the observed star formation rate using equation (16) is overestimated by the ratio of $(dt/dz\Delta z)$ to the starburst lifetime. However, in contrast to observations at $z \sim 2-4$, at $z > 6$ we expect that the observed galaxies did star form of a time equal to the survey depth, meaning that the stellar mass census does include all the stellar mass that was generated during the survey depth time interval. As a result, in the $z > 6$ samples equation (16) does give a stellar mass that approximately equals the mass observed in those $z \sim 6$ galaxies, in agreement with the comparison of Bouwens et al. (2011) This equivalence is a coincidence, and does not correspond to a large duty cycle. Galaxies not star forming and therefore not seen in the survey did not form stars during that time in this case. As in the $z \sim 2-4$ case, this implies that there is additional stellar mass in quiescent galaxies that is not accounted for in the observed stellar mass function.

We note that if the galaxy sample were selected on stellar mass rather than on UV luminosity, the estimates of star formation rate density based on instantaneous SFRD and the derivative of stellar mass density would agree.

REFERENCES

Barkana R., Loeb A., 2001, ApJS, 349, 125
Bell E. F., de Jong R. S., 2001, ApJ, 550, 212
Bouwens R. J., Illingworth G. D., Oesch P. A., Labbé I., Trenti M., van Dokkum P., Franx M., Stiavelli M., Carollo C. M., Magee D., Gonzalez V., 2011, ApJ, 737, 90
Clarke C., Oey M. S., 2002, MNRAS, 337, 1299
Dekel A., Woo J., 2003, MNRAS, 344, 1131
Finlator K., Oppenheimer B. D., Davé R., 2011, MNRAS, 410, 1703
Gonzalez V., Bouwens R., llingworth G., Labbe I., Oesch P., Franx M., Magee D., 2012, ArXiv e-prints
González V., Labbé I., Bouwens R. J., Illingworth G., Franx M., Kriek M., 2011, ApJL, 735, L34
Jaacks J., Nagamine K., Choi J.-H., 2012, ArXiv e-prints
Kauffmann G., Heckman T. M., White S. D. M., Charlot S., Tremonti C., Peng E. W., Seibert M., Brinkmann J., Nichol R. C., SubbaRao M., York D., 2003, MNRAS, 341, 54
Komatsu E., Smith K. M., Dunkley J., Bennett C. L., Gold B., Hinshaw G., Jarosik N., Larson D., et al. 2011, ApJS, 192, 18
Lacey C., Cole S., 1993, MNRAS, 262, 627
Lee K.-S., Ferguson H. C., Wiklind T., Dahlen T., Dickinson M. E., Giavalisco M., Grogin N., Papovich C., Messias H., Guo Y., Lin L., 2012, ApJ, 752, 66
Lee K.-S., Giavalisco M., Conroy C., Wechsler R. H., Ferguson H. C., Somerville R. S., Dickinson M. E., Urry C. M., 2009, ApJ, 695, 368
Mo H. J., Mao S., White S. D. M., 1998, MNRAS, 295, 319
Muñoz J. A., Loeb A., 2011, ApJ, 729, 99
Neistein E., Dekel A., 2008, MNRAS, 383, 615
Oey M. S., Clarke C. J., 1997, MNRAS, 289, 570
Press W. H., Schechter P., 1974, ApJ, 187, 425
Raičević M., Theuns T., Lacey C., 2011, MNRAS, 410, 775
Salvaterra R., Ferrara A., Dayal P., 2011, MNRAS, 414, 847
Scalo J., 1998, in Gilmore G., Howell D., eds, The Stellar Initial Mass Function (38th Herstmonceux Conference) Vol. 142 of Astronomical Society of the Pacific Conference Series, The IMF Revisited: A Case for Variations. p. 201
Sheth R. K., Tormen G., 1999, MNRAS, 308, 119
Smit R., Bouwens R. J., Franx M., Illingworth G. D., Labbé I., Oesch P. A., van Dokkum P. G., 2012, ArXiv e-prints
Trenti M., Stiavelli M., Bouwens R. J., Oesch P., Shull J. M., Illingworth G. D., Bradley L. D., Carollo C. M., 2010, ApJL, 714, L202
Weinmann S. M., Neistein E., Dekel A., 2011, MNRAS, 417, 2737
Wilkins S. M., Trentham N., Hopkins A. M., 2008, MNRAS, 385, 687
Wyithe J. S. B., Loeb A., 2003, ApJ, 595, 614
Wyithe J. S. B., Loeb A., 2013, MNRAS, 428, 2741